physica status solidi

pss

www.pss-journals.com

reprint

WILEY-VCH

Phys. Status Solidi B **252,** No. 1, 139–143 (2015) / **DOI** 10.1002/pssb.201400116

physica status solidi b
www.pss-b.com
basic solid state physics

Confinement effects for the *F* center in non-stoichiometric $BaZrO_3$ ultrathin films

Marco Arrigoni*[,1], Eugene Kotomin[1,2], Denis Gryaznov[**,2], and Joachim Maier[1]**

[1] Max Planck Institute for Solid State Research, Heisenbergstraße 1, 70569 Stuttgart, Germany
[2] Institute of Solid State Physics, University of Latvia, Kengaraga 8, 1063 Riga, Latvia

Received 23 May 2014, revised 11 July 2014, accepted 14 July 2014
Published online 1 December 2014

Keywords *ab initio* calculations, $BaZrO_3$, oxygen vacancy, phonons, thin films

* Corresponding author: e-mail m.arrigoni@fkf.mpg.de, Phone: +49 711 689 1738, Fax: +49 711 685 1722
** e-mail gryaznov@mail.com, Phone: +371 6718 7480

First principles calculations of the atomic, electronic structure, and phonons frequencies were performed to investigate confinement effects on the oxygen vacancy (the *F* color center) in $BaZrO_3$ ultrathin films. The defect was considered both inside the films and on the (001) surface with BaO and ZrO_2 terminations. We consider the effects of the one-dimensional confinement through varying the number of planes in the films from 3 to 9 and comparing the results with those obtained for the bulk material. We have studied how the one-dimensional confinement affects the electronic properties (band structure, Mulliken atomic charges) and the phonon frequencies of the defective systems, and thus how the defect formation energy in thin films at finite temperatures is affected as compared with the bulk material.

1 Introduction In this short paper we consider the effects of the one-dimensional confinement on the energetic, electronic, and thermodynamic properties of perovskite thin films containing the color *F* centers (an oxygen vacancy with two trapped electrons: $V_O^{\times}$ in the Kröger–Vink nomenclature [1]) in a comparison with the bulk defect. We focused our attention on three main effects that could arise from the dimensional confinement: the localization of the defect wave function, the restricted relaxation volume available for the surrounding ions and the confinement of lattice vibrations within thin films.

We consider $BaZrO_3$ as a prototype for a wide class of cubic ABO_3-type perovskites (space group $Pm\bar{3}m$). The oxygen vacancies are very common defects in perovskites and understanding their properties in very thin films is important for many applications, such as new switching resistive memories [2], nano-capacitators [3, 4], spintronics [5], and proton conducting fuels cells [6]. When an oxygen ion is removed from the regular lattice site, the surrounding lattice is relaxed and two electrons remaining from a missing O^{2-} ion are redistributed between a vacancy and nearest ions, in order to achieve minimum of the total energy.

So far a number of first principles studies were performed for oxygen vacancies in $BaZrO_3$ (*e.g.* [7]) and $SrTiO_3$ (*e.g.* [8]) but not in thin films. On the other hand, the first study of confinement effects was recently performed for the *F* centers in thin films of $SrTiO_3$ [9]). It was shown that the effects are expected to be short-range, limited to the nm-thick thin films. We extend this study methodologically, taking into account the phonon contribution into the free energy for defect formation at realistic temperatures where devices are operating.

2 Method We performed the linear-combination-of-atomic-orbitals (LCAO) *ab initio* calculations within the HF-DFT hybrid approximation applying periodic boundary conditions. The hybrid Perdew–Burke–Ernzerhof (PBE0) exchange-correlation functional [10] was used as implemented in the CRYSTAL09 computer package [11].

We rely on a supercell model in our simulations of defect behavior in the bulk material and the thin films. To avoid excessive interaction between the defect and its spurious images in bulk material, we used a $3 \times 3 \times 3$ expansion (135 atoms) of 5-atom primitive unit cell, thus, corresponding to a vacancy concentration of 3.70%. Due to computational costs we calculated the vibrational modes of the bulk material employing a smaller supercell ($2 \times 2 \times 2$ expansion, containing 40 atoms).

Thin films were modeled using the slabs with a two-dimensional periodicity and a 3×3 square lattice expansion.

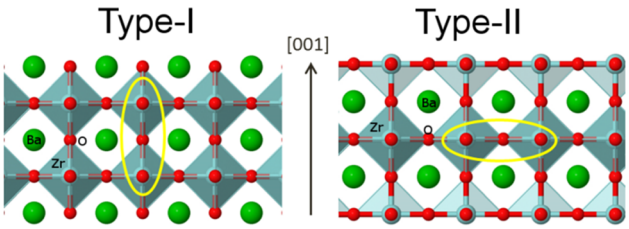

Figure 1 Graphic representation of type-I and type-II films. In the first case the central plane has composition BaO whereas in the latter ZrO_2. The orientation of the Zr–O(V_O)–Zr defect complex is underlined.

We considered the (001) slabs symmetrical on both sides, containing from 3 to 9 layers (with an odd number of planes, to exploit in the calculations the symmetry brought by the reflection plane situated in the slab central layer), thus, corresponding to non-stochiometric free-standing films with a thickness varied roughly between 0.4 and 1.7 nm. We considered both kinds of possible termination layers (BaO and ZrO_2 planes). We call, hereafter, the films as *type-I* or *type-II* depending if the central plane composition is BaO or ZrO_2, respectively, see Fig. 1.

We used a $3 \times 3 \times 3$ and a 3×3 Monkhorst-Pack mesh of *k*-points in the Brillouin Zone [12], respectively, for bulk and thin films. The basis set of $BaZrO_3$ was optimized in the previous study [13]. It consisted of Gaussian-type functions and pseudopotentials for Ba and Zr taken from pseudopotential library of Stuttgart/Cologne group [14]. In contrast, the all-electron basis set was used for oxygen. We studied the defective systems in the singlet state since our preliminary calculations on the bulk $BaZrO_3$ have shown that the triplet state lies much higher (1.14 eV) in energy than singlet. The geometry of both bulk and $BaZrO_3$ films was fully optimized, relaxing both cell parameters and atomic coordinates.

With this computational setup, we reproduced correctly the experimental band gap of the material; the result is important for the study of defects, as oxygen vacancies in ABO_3 perovskites, that originate levels inside this gap. The calculated gap of 5.36 eV was in a very good agreement with the experimental one (5.33 eV) [15]. We reproduced correctly also the bulk lattice constant: the computed value of 4.195 Å is very close to the value of 4.192 Å found in experiments [16]. The Mulliken population analysis shows the bonding character in $BaZrO_3$ has a consistent covalent contribution (q(Ba) = 1.66 e, q(Zr) = 2.35 e, q(O) = −1.33 e).

To describe possible localization of the electronic density within the oxygen vacancy, we kept there the basis ("ghost") functions of the missing O atom.

The *F* centers were considered in both the bulk and in thin films – in the central plane and on slab surfaces. In the surface defect study, we removed *two* oxygen atoms from the opposite surfaces, to fully exploit the symmetry of the system. We calculated the *formation energy* of the defect at zero temperature (zero-point energy excluded) as a function of the film thickness using the standard expression:

$$\Delta E_f = \frac{1}{n}\left(E^{\mathrm{def}} - E^{\mathrm{perf}} + \frac{n}{2}E^{\mathrm{O_2}}\right), \tag{1}$$

where E^{def} represents the total electronic energy of the defective system containing n oxygen vacancies (in our case $n = 2$ in the films where the *F* center is considered on the slab surfaces; in all the other cases $n = 1$), E^{perf} is the total electronic energy of the perfect system and $E^{\mathrm{O_2}}$ the total electronic energy of a free oxygen molecule in its triplet ground state.

To take into account the effects of the finite temperature, we calculate the phonon frequencies in the harmonic approximation at the Γ-point of the Brillouin zone. The dynamical matrix is obtained by computing numerically the first derivative of the atomic energy gradients [17] displacing the atoms along the Cartesian coordinates by steps of 0.001 Å.

We performed the calculation at the constant pressure of one atmosphere for systems containing one oxygen vacancy in the bulk and in the central plane of the thin films, and then we calculated the formation energy of the *F* center at finite temperatures according to the relation:

$$\Delta A_f(T) = A^{\mathrm{def}}(T) - A^{\mathrm{perf}}(T) + \mu_{\mathrm{O}}(T), \tag{2}$$

where $A^{\mathrm{def}}(T)$ and $A^{\mathrm{perf}}(T)$ are the Helmholtz energies for the system containing the oxygen vacancy and the perfect one, respectively, and μ_{O} is the chemical potential of an oxygen atom (half the energy of an oxygen molecule: $\mu_{\mathrm{O}}(T) = 1/2\,A_{\mathrm{O_2}}(T)$ corresponding to the case of an oxygen rich atmosphere). Notice that in our systems the relaxation volumes relative to the introduction of the F center are very small, thus the $p\Delta V$ term in the Gibbs free energy of formation is completely negligible and the value of $\Delta A_f(T)$ should be very similar to that of $\Delta G_f(T)$.

3 Results and discussions

3.1 Properties of the *F* center in bulk and the center of thin films The *F* center does not affect much the geometry of the bulk material: the nearest Zr cations are displaced outwards by $<1\%$ a_0. The Mulliken population analysis [18] shows that the vacancy traps one electron ($q(\mathrm{V_O}) = -1.03$ e); while another electron is delocalized, mainly on the nearest cations. In the supercell used the defect creates a new occupied band in the gap with a width (dispersion) $\delta = 0.14$ eV being located by $\Delta\varepsilon = 1.63$ eV below the conduction band at the Γ-point. This is in agreement with previous observation that the *F*-center in zirconates are deep defects [19], unlike in $SrTiO_3$ ([8]).

In thin films with one oxygen vacancy in the central plane, the local atomic structure around the vacancy differs from that discussed for the bulk only for the thinnest films made of just three lattice planes for both type-I and type-II

Table 1 Geometrical parameters for the *F* center in bulk and in the central plane of $BaZrO_3$ thin films. The displacements with respect to the perfect system (Δd in Å) are reported for the oxygen vacancy and its neighbors in the first three coordination shells. A negative Δd means an inward relaxation. The data are displayed as a function of the number of planes (*N*) and the type of termination plane (T) for type-I, type-II films, and bulk $BaZrO_3$.

type-I *N*/T	$\Delta d(V_O–Zr)$	$\Delta d(V_O–Ba)$	$\Delta d(V_O–O)$
3/ZrO_2	−0.14	0.03	−0.12
5/BaO	0.06	−0.02	−0.01
7/ZrO_2	−0.02	0.00	−0.05
9/BaO	0.01	0.00	−0.03
BULK	0.00	0.00	−0.03
type-II *N*/T	$\Delta d(V_O–Zr)$	$\Delta d(V_O–Ba)$	$\Delta d(V_O–O)$
3/BaO	−0.15	0.05	−0.17
5/ZrO_2	−0.02	0.00	−0.04
7/BaO	−0.03	0.00	−0.04
9/ZrO_2	−0.02	0.00	−0.04
BULK	0.00	0.00	−0.03

films. As Table 1 shows, the distances between V_O and its neighbors in the first three coordination shells converge rapidly to the bulk value; only in 3-plane films the Zr–V_O and O–V_O distances are distinctly shorter (≈10% for Zr–V_O and ≈7% for O–V_O), indicating that practically confinement effects on the local structure of the *F* center are minimal.

The Mulliken population analysis (Table 2) shows also that effective charge deviations from the bulk are considerable only for very thin films: 3,5-plane type-I and 3-plane for type-II. This shows also that the type of termination plane and the orientation of the Zr–V_O–Zr complex have some effects on the electronic structure. In fact, type-I 5-plane film (the Zr–V_O–Zr complex (Fig. 1) is oriented perpendicularly to the surface) and type-II 3-plane film (Zr–V_O–Zr parallel to the surface) have the same termination layer (BaO surfaces), but for the former the vacancy population is less than in the bulk due to the electronic delocalization toward nearest cations, while for the latter the vacancy population is larger due to a charge transfer from the nearest Zr atoms. We do not notice a dependence of the vacancy population with respect to the orientation of the Zr–V_O–Zr complex when the termination layer is a ZrO_2 surface.

Table 2 Electronic structure characteristics for the *F* center in bulk and in the central plane of type-I and type-II thin films. $\Delta\varepsilon$ indicates the distance of the defective level with respect to the conduction band minimum at the Γ-point, $\delta\varepsilon$ is the width of this band in the gap. The Mulliken charges for the vacancy and its first Zr neighbors are also reported. *N* is the number of planes in the slab and T the termination plane.

type-I *N*/T	$\Delta\varepsilon$ (eV)	$\delta\varepsilon$ (eV)	Mulliken charges (*e*)	
			V_O	Zr
3/ZrO_2	3.10	0.01	−1.09	2.30
5/BaO	1.42	0.01	−0.93	2.37
7/ZrO_2	1.96	0.01	−1.03	2.37
9/BaO	1.83	0.11	−1.00	2.38
BULK	1.63	0.14	−1.03	2.39
type-II *N*/T	$\Delta\varepsilon$ (eV)	$\delta\varepsilon$ (eV)	Mulliken charges (*e*)	
			V_O	Zr
3/BaO	2.48	0.13	−1.16	2.47
5/ZrO_2	1.65	0.15	−1.04	2.38
7/BaO	1.83	0.11	−1.06	2.40
9/ZrO_2	1.73	0.11	−1.04	2.34
BULK	1.63	0.14	−1.03	2.39

Table 2 also shows the position ($\Delta\varepsilon$) of the defective band respectively the bottom of the conduction band and its width ($\delta\varepsilon$) in the gap. The defective level oscillates around the bulk value of 1.63 eV for both kind of thin films, and it lies considerably deeper in the thinnest 3-plane films. The width of the band is affected by the orientation of the Zr–V_O–Zr complex; flatter bands occur in the type-I films, but starting from nine layers and more the band width saturates to the bulk value found in the $3 \times 3 \times 3$ supercell.

Only for 3-plane slabs the formation energy of the *F* center in the central plane of thin films, Eq. (1), differs considerably (≈0.5 eV) from that in the bulk (6.97 eV), see Fig. 2. Thus, the confinement effects at low temperatures are very-short ranged and noticeable only for very ultrathin films (three planes); this depends slightly on the orientation of the Zr–V_O–Zr complex with respect to the film surface (parallel or perpendicular). Note that a large contribution to ΔE_f comes from the complete film structure relaxation. In the 3-plane slabs the structure relaxation lowers the formation energy of the type-I films by 0.6 eV whereas for the type-II by 0.9 eV. These values increase greatly when the number of

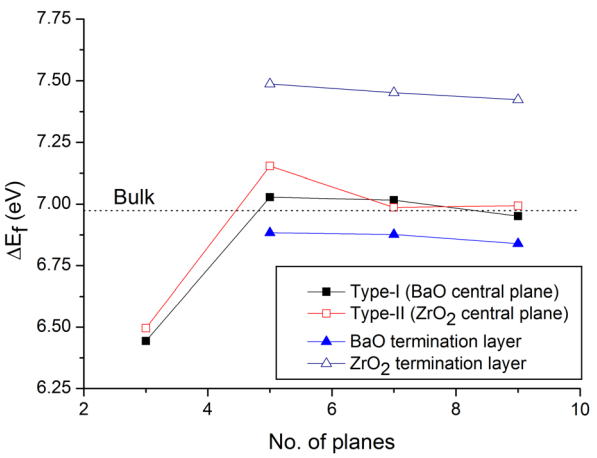

Figure 2 Formation energy of the *F* center in $BaZrO_3$ thin films as a function of the film thickness. The squares correspond to oxygen vacancies in the center of the films, while the triangles to oxygen vacancy on the film surfaces (see legend for details). The dashed line shows the defect formation energy in the bulk.

Table 3 Structural parameters for the *F* center on the surface. *d* is the distance (in Å) between the vacancy and its neighbors in the first three coordination shells. The data are given as a function of plane numbers (*N*) in a slab for BaO and ZrO_2 terminations.

BaO surface	$d(V_O–Zr)$	$d(V_O–Ba)$	$d(V_O–O)$
5	2.49	3.05	3.13
7	2.48	3.05	3.13
9	2.48	3.05	3.13
ZrO_2 surface	$d(V_O–Zr)$	$d(V_O–Ba)$	$d(V_O–O)$
5	2.18	3.22	2.96
7	2.19	3.18	2.96
9	2.19	3.16	2.97

layers is equal or larger than five; in this case the *F* center formation energy is reduced by ~2 eV, being slightly higher for the BaO termination.

3.2 Properties of the *F* centers on the surface of thin films The local lattice distortion around the surface *F* centers is affected by the chemical nature of the terminating plane containing the defect but is rather insensitive to the film thickness (Table 3), indicating very short-range interactions between the *F* center and its surroundings.

We have also calculated the formation energy of oxygen vacancies on the surface of $BaZrO_3$ films, as previously described. The results shown in Fig. 2 and are compared with those obtained for the *F* center in the bulk and in the central plane of the slabs.

It can be seen that the surface defect formation energy is rather insensible to the film thickness. However, the formation energy for the BaO termination is smaller than for the ZrO_2 termination whereas the formation energy for the bulk is in-between. In other words, we predict that the *F* centers tend to migrate from the bulk toward BaO surfaces but not to ZrO_2 ones.

Table 4 shows the positions of the defective levels with respect to the conduction band in films with different termination layers. We can see that oxygen vacancies on the BaO surface induce deeper defective bands (≈0.2 eV) than vacancies on the ZrO_2 termination. We can also notice that when oxygen vacancies are placed on the more ionic surface (BaO), the defective band is split in two in 5-plane and 7-plane films. This means that the interaction of the oxygen vacancies placed on the opposite BaO surfaces is completely shielded only in thick films.

Note that in all cases the surface *F* centers creates deep defects, similar as in the bulk. This is in agreement with the *F* center calculations in other zirconates [19].

3.3 Contribution of phonons to the defect formation energy In order to consider realistic external conditions, we performed phonon calculations. We calculated the lattice vibration frequencies and the vacancy formation energy for the 3-plane and 5-plane films of type-I containing the *F* center in their central plane and compared with those obtained for the $BaZrO_3$ bulk.

To emphasize the contribution of phonons to the defect formation energy, we have plotted in Fig. 3 two types of curves. The solid curves are obtained plotting the formation energy, as given by Eq. (2), with complete incorporation of the phonon contribution as a function of the temperature; while for dashed curves the defect formation energy was plotted taking into account the temperature dependence of the oxygen chemical potential only.

We can see that the contribution of phonons to the *F* center formation energy is essential only at high temperatures. For example, at 1000 K the formation energy is increased by 0.1 eV in the bulk, by 0.03 eV in 5-plane film and by 0.2 eV in 3-plane films. The difference between the bold and dashed curves gives us the vibrational contribution to the Helmholtz (Gibbs) defect formation energy:

$$\Delta A_{\mathrm{vib}}(T) = \Delta U_{\mathrm{vib}}(T) - T\Delta S_{\mathrm{vib}}(T). \quad (3)$$

Table 4 The electronic structure of the *F* center on the two different surfaces. The Mulliken charges (in units of the elementary charge *e*) on the oxygen vacancy and its nearest Zr neighbors, the position of the defective levels in the band gap ($\Delta\varepsilon$) and their dispersion in the reciprocal space ($\delta\varepsilon$) are given.

BaO surface	Mulliken charges		$\Delta\varepsilon$ (eV)		$\delta\varepsilon$ (eV)	
	V_O	Zr				
5	−0.74	2.30	1.01	1.33	0.01	0.01
7	−0.74	2.31	1.09	1.15	0.01	0.01
9	−0.74	2.31	1.10		0.02	
ZrO_2 surface	Mulliken charges		$\Delta\varepsilon$ (eV)		$\delta\varepsilon$ (eV)	
	V_O	Zr				
5	−0.88	2.29	1.04		0.02	
7	−0.89	2.29	0.94		0.02	
9	−0.89	2.29	0.89		0.02	

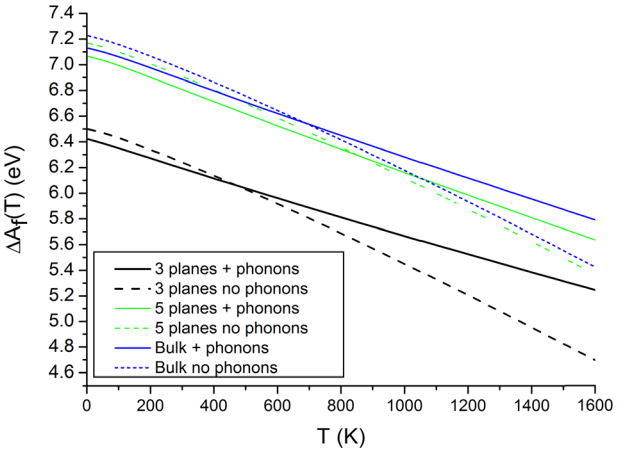

Figure 3 Oxygen vacancy formation energies as a function of the temperature calculated for bulk, 3- and 5-layer type-I films. For the bold lines the formation energy was calculated including phonons, Eq. (2), dashed lines incorporate only the oxygen chemical potential.

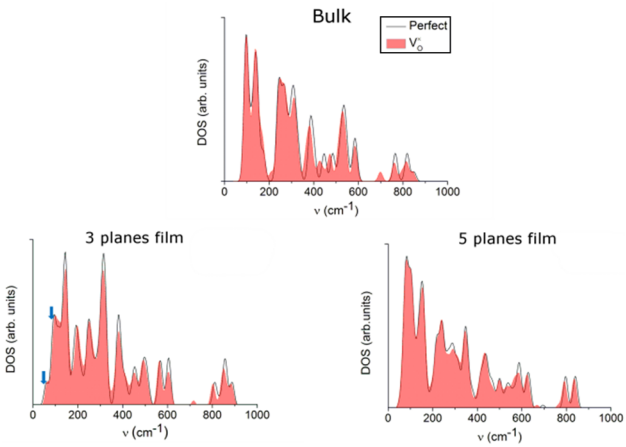

Figure 4 Density of states of phonon frequencies in the bulk and type-I thin films. The empty curves represent the PDOS for the perfect systems and the filled curves for those containing the *F* center. The blue arrows indicate the slight shift toward higher frequencies for the first normal modes in 3-plane films.

This term is particularly relevant for the 3-plane films. This can be explained by analysis of Fig. 4, with a comparison of the phonon density of states (PDOS) for thin films and the bulk. Looking at the differences between the empty curve for the perfect system's PDOS, and those for the defective system, we notice for 3-plane films a slight shift of the frequencies of the low frequency normal modes toward higher frequencies (blue arrows). This shift decreases the *entropy* of the defective system and thus $\Delta A_{\mathrm{vib}}(T)$ increases. The shift toward higher frequencies in the PDOS could be explained from data in Table 1. For 3-plane films the vacancy neighbors are displaced toward the vacancy; as a consequence there is a compression of their bonds that causes stronger interatomic forces and thus slightly higher vibrational frequencies. This does not happen in bulk and thicker films since in this case the distorsions around the *F* center are very modest.

4 Summary We compared the local atomic and electronic structure and the frequencies of the lattice vibrations in thin films and bulk $BaZrO_3$ with the color *F* center.

For defects located on the film surface the energetic, geometric, and electronic properties are not practically affected by the film thickness. For oxygen vacancies in thin film center the confinement effects are very short-ranged even with entropy contribution and are relevant only in 3-layer films. In particular, the confinement is responsible for the deeper defect levels position in the gap, and for larger geometric distorsions of the surrounding lattice. The latter is responsible for a slight shift of phonon frequencies toward larger values that slightly increases the defect formation energy.

Acknowledgements Authors are indebted to R. Merkle, Yu. F. Zhukovskii, E. Heifets, and T. S. Bjørheim for many stimulating discussions. D. G. was supported by ESF grant No. 2013/0046/1DP/1.1.1.2.0/13/APIA/VIAA/021, E. K. by COST Action CM1104. Most of calculations were performed in the Stuttgart Supercomputing Center (HLRS Project DEFTD 12939).

References

[1] F. Kröger and H. Vink, Solid State Phys. **3**, 307 (1956).
[2] R. Waser and M. Aono, Nature Mater. **6**, 883 (2007).
[3] D. D. Fong, G. B. Stephenson, S. K. Streiffer, J. A. Eastman, O. Auciello, P. H. Fuoss, and C. Thompson, Science **304**, 1650 (2004).
[4] C. Foerst, Nature **427**, 53 (2003).
[5] K. Wang, Y. Ma, and K. Betzler, Phys. Rev. B **76**, 144431 (2007).
[6] K. Kreuer, Annu. Rev. Mater. Res. **33**, 333 (2003).
[7] P. Sundell, M. Björketun, and G. Wahnström, Phys. Rev. B **73**, 104112 (2006).
[8] R. Evarestov, E. Blokhin, D. Gryaznov, E. A. Kotomin, R. Merkle, and J. Maier, Phys. Rev. B **85**, 174303 (2012).
[9] E. A. Kotomin, V. Alexandrov, D. Gryaznov, R. A. Evarestov, and J. Maier, Phys. Chem. Chem. Phys. **13**, 923 (2011).
[10] J. P. Perdew, M. Ernzerhof, and K. Burke, J. Chem. Phys. **105**, 9982 (1996).
[11] R. Dovesi, V. Saunders, C. Roetti, R. Orlando, C. M. Zicovich-Wilson, F. Pascale, B. Civalleri, K. Doll, N. M. Harrison, I. J. Bush, Ph. D'Arco, M. Llunel, M. Causà, and Y. Noël, CRYSTAL09 User's Manual (2013).
[12] H. J. Monkhorst and J. D. Pack, Phys. Rev. B **13**, 5188 (1976).
[13] R. A. Evarestov, Phys. Rev. B **83**, 014105 (2011).
[14] Available online at: http://www.theochem.uni-stuttgart.de/pseudopotentials/clickpse.html.
[15] J. Robertson, J. Vac. Sci. Technol. B **18**, 1785 (2000).
[16] W. Pies and A. Weiss, Landolt-Börnstein: Numerical Data and Functional Relationship in Science and Technology (Springer, Berlin, 1975).
[17] F. Pascale, C. M. Zicovich-Wilson, F. López Gejo, B. Civalleri, R. Orlando, and R. Dovesi, J. Comput. Chem. **25**, 888 (2004).
[18] R. Mulliken, J. Chem. Phys. **23**, 1833 (1955).
[19] Yu. F. Zhukovskii, E. A. Kotomin, S. Piskunov, and D. E. Ellis, Solid State Commun. **149**, 1359 (2009).